Differential cross sections for pion charge exchange on the proton at 27.5 MeV

E. Frlež, D. Počanić, K. A. Assamagan,* J. P. Chen,† K. J. Keeter,‡ R. M. Marshall, R. C. Minehart, and L. C. Smith
Department of Physics, University of Virginia, Charlottesville, Virginia 22901

G. E. Dodge,§ S. S. Hanna, and B. H. King
Department of Physics, Stanford University, Stanford, California 94305

J. N. Knudson
Los Alamos National Laboratory, Los Alamos, New Mexico 87545
(Received 17 December 1997)

We have measured pion single charge exchange differential cross sections on the proton at 27.5 MeV incident π^- kinetic energy in the center of momentum angular range between 0° and 55°. The extracted cross sections are compared with predictions of the standard pion-nucleon partial wave analysis and found to be in excellent agreement. [S0556-2813(98)00506-8]

PACS number(s): 25.80.Gn, 11.80.Et, 13.75.Gx

I. INTRODUCTION

Absolute measurements of the pion-nucleon differential scattering cross sections below 150 MeV are sparse. The experimental database for the pion single charge exchange reaction on the nucleon (πN SCX) at these low energies is quite limited. The most recent pion-nucleon partial-wave analyses by Arndt *et al.* [1,2] reflect that paucity of data. Their parametrizations neglect the expected isospin breaking effects and the interesting physics that could lie beyond the hadronic mass differences and the Coulomb interaction [3]. The data for the SCX reaction on free nucleons are, in addition, essential for our understanding of nuclear medium effects on the πN interaction [4], such as multiple scattering processes and valence nucleon densities.

The question of the magnitude of the ''sigma term'' matrix element is also not yet settled. The πN σ term explicitly breaks chiral symmetry in the effective QCD Lagrangian. Extrapolation of $\bar{D}^+$, an isospin-even πN scattering amplitude, to the nonphysical region leads to a value that is significantly larger than that extracted from the baryon mass spectra. The difference has been attributed to a nonzero $\bar{s}s$ quark content of the nucleon [5]. Inconsistencies between different πN scattering experiments have impeded an unambiguous resolution of that discrepancy for a long time [6,7].

The principal experimental difficulties in measuring the πN SCX process below 150 MeV arise from the need for an accurate determination of the beam composition, absolute beam flux normalization, and accurate calibration of the π^0 detection efficiency. Two techniques have been used in the past to measure the πp SCX differential cross sections. Early experiments [8,9] used NaI crystal counters to detect a single photon from the final state π^0 decay, deducing the π^0 angular distribution from the energy spectrum of the accepted γ rays. These measurements were performed at eight incident π^- energies between 26.4 and 121.9 MeV and covered the laboratory polar angles between 0° and 145°. The experimental uncertainties ranged from over 150% at low energies and forward angles, to about 6% at energies above 40 MeV and scattering angles larger than 60°.

Other published data [10] come from a study that used the LAMPF π^0 spectrometer for the coincident detection of two π^0 photons. This measurement was made at seven beam energies between 32.5 and 63.5 MeV and was restricted to laboratory polar angles smaller than 30°. In a later LAMPF experiment Sadler *et al.* used an electrostatic separator to obtain a pure pion beam in the energy range 10–40 MeV covering a selection of forward and backward center-of-momentum scattering angles; their preliminary results are reported in Ref. [11].

Details of our experimental technique are given below. In Sec. II we discuss the critical issue of the π^- beam contamination which is large at low energies, and show how we extracted the electron and muon beam fractions from the measurements. Section III specifies the composition, dimensions, and geometry of the targets and the effective beam energies on targets. The integrated efficiency of the π^0 detector, discussed in Sec. IV, is broken into several factors whose values are determined in both calibration measurements and in a Monte Carlo simulation. The experimental cross sections are presented in Sec. V where they are compared with the partial-wave analysis prediction and previously published data.

II. BEAM COMPOSITION AND FLUX NORMALIZATION

The measurements were performed in the Low-Energy Pion (LEP) channel at the Clinton P. Anderson Meson Physics Facility (LAMPF) [12]. A weakly focusing 30 MeV π^- beam tune was developed with 12 mr horizontal and vertical divergences, near-circular beam spot with a diameter of 9

*Present address: Physics Department, Hampton University, Hampton, VA 23668.
†Thomas Jefferson National Accelerator Facility, Newport News, VA 22606.
‡Present address: Department of Physics, Idaho State University, Pocatello, ID 83209.
§Present address: Department of Physics, Old Dominion University, Norfolk, VA 22606.

TABLE I. Recommended $^{12}C(\pi^-,\pi N)^{11}C$ activation cross sections for 30, 40, and 50 MeV $\pi^\pm$ beams and cross sections for ^{11}C production by electrons of the same momenta from unpublished measurements of Leitch *et al.* [16]. The e^- activation cross section σ_{e^-} at 128 MeV/ c was published by Kuhl and Kneissl [17]. The μ^+-induced ^{11}C production measured with a 60 MeV μ^+ beam gave five hundred times smaller cross sections than the associated π^+ activity [18]. Consequently, the activation cross sections weighted over the π^- beam momentum spread in the activation target disk used in our analysis were $\sigma_{\pi^-}(\overline{T}_{\pi^-}=28.7$ MeV$)=1.50\pm0.07$ mb, $\sigma_{e^-}(\overline{T}_{e^-}=94.6$ MeV$)=64.4\pm3.4$ μb, and $\sigma_{\mu^-}(\overline{T}_{\mu^-}=36.2$ MeV$)=9.1\pm1.7$ μb, respectively. The fifth column shows the ratio of the unpublished π^--induced activation cross sections from the LAMPF experiment E942 to the older values that were used for π^- beam flux normalization in the πp SCX experiment of Ref. [10].

p_{beam} (MeV/ c)	$T_{\pi^\pm}$ (MeV)	σ_{π^+} (mb)	σ_{π^-} (mb)	$\frac{\sigma_{\pi^-}\text{Ref. [16]}}{\sigma_{\pi^-}\text{Ref. [29]}}$	σ_{e^-} (mb)
17.3	18.7	0.0	0.0	0.0	0.0
96.3	30.0	3.2 ± 0.4	1.70 ± 0.08	1.89	0.0664 ± 0.0035
113.0	40.0	6.5 ± 0.4	3.89 ± 0.15	1.34	0.0954 ± 0.0140
128.3	50.0	10.3 ± 0.6	6.10 ± 0.50	1.00	0.124 ± 0.020

mm full width at half maximum (FWHM) at target location, momentum spread $\Delta p/p$ of 3%, and pion flux averaging 6×10^5 π^-/sec.

Relative on-target beam intensity was monitored with a gas ion chamber in combination with a precision charge integrator. The chamber was a sealed 30 cm long aluminum cylinder with 125 μm steel windows, filled with 0.0427 g/cm^2 of argon gas.

Absolute cross-calibration of chamber ionization counts against the number of pions in the beam was obtained through activation measurements of the $^{12}C(\pi^-,\pi N)^{11}C$ reaction using $\phi70$ mm$\times$3.2 mm disk-shaped plastic scintillator targets (PILOT B scintillator, 91.6% ^{12}C by weight) [13]. The ^{11}C activity of these targets, measured after exposures to the π^- beam of typically 20 minute duration (one half-life of ^{11}C) was well above background counting rates. The background rates in the irradiated disks were constrained separately in the analysis of each activation by independently measured e^+-γ detection efficiencies of the ^{11}C counting apparatus. The positron, photon, and the coincident e^+-γ signal were on average six, three, and one hundred times the background levels, respectively. Polaroid films irradiated during the beam activations showed ellipsoidal beam spots with major axes $\Delta x\times\Delta y=5\times3$ cm^2 fully contained within the activation disk areas. The focused beam pions, muons, and electrons coming from the production target produced overexposed beam spots, while the muons from pions decaying in flight left only a weak 10 cm diameter halo on Polaroid films placed at the target position. The statistical reproducibility of the method outlined above was better than 2.0%.

The absolute calibration of the ion chamber was performed using higher momentum π^+'s during our study of the $\pi^+p\rightarrow\pi^0\pi^+p$ process near threshold [14], i.e., the ratio of ionization counts I_c to the electron-equivalent energy ΔE_{ee} deposited in the chamber gas was determined using ionizing particles in 160–260 MeV π^+ beams. Energy depositions of different charged particles were calculated using the Bethe-Bloch formula with appropriate corrections [15]. Protons in the π^+ beams were suppressed by means of a thin degrader in the beam line. The residual proton fraction $f_p=N_p/N_{\pi^+}$ was deduced by two independent methods: (i) a coincident pp scattering using a liquid H_2 target of known thickness in conjunction with the published differential pp cross sections [1], and (ii) π^+p momentum separation scans. In the momentum scan measurements the ionization count rate was determined as a function of the magnetic fields of the channel dipole magnets and quadrupoles downstream of the thin degrader, covering a 10% range around the nominal momentum setting and thus allowing easy mapping of the proton and pion beam momentum profiles. The proton contaminations f_p of the π^+ beam tunes used for the ion chamber calibration were found to be stable at $0.6\pm0.1\%$. The ratio $I_c/\Delta E_{ee}$ characterizing the ion chamber was established to be $(2.57\pm0.11)\times10^{-5}$ counts/MeV$_{ee}$.

The activation measurements were affected by non-pionic contaminations of the beam, i.e., electrons and muons. The apparent number of π^-'s deduced from the activation measurements using the 96 MeV/c incident beam, with the electron contamination $f_{e^-}=N_{e^-}/N_{\pi^-}$ and the muon contamination $f_{\mu^-}=N_{\mu^-}/N_{\pi^-}$, had to be reduced by the factor

$$1+f_{e^-}\frac{\sigma_{e^-}}{\sigma_{\pi^-}}+f_{\mu^-}\frac{\sigma_{\mu^-}}{\sigma_{\pi^-}}, \tag{2.1}$$

where σ_{e^-}, σ_{μ^-}, and σ_{π^-} are the e^-, μ^- and π^- ^{11}C activation cross sections, respectively. The unpublished recommended low energy e^- and $\pi^\pm$ activation cross sections [16] used in our analysis are listed in Table I for the 30, 40, and 50 MeV incident $\pi^\pm$ beams. The cross section for the ^{12}C $(\mu^+,\mu^+n)^{11}C$ reaction with a 60 MeV μ^+ beam is known to be 21 ± 4 μb [17,18]. Since $\mu^\pm$ activation cross sections are essentially charge independent we have used this datum in the absence of a μ^- measurement. The incident particle threshold energy below which the ^{11}C activation cross section has to be zero is 18.7 MeV. Using all of the above data we obtained interpolated values of ^{11}C activation cross sections at energies appropriate for our activation measurements. These values, used in our analysis, are also given in Table I.

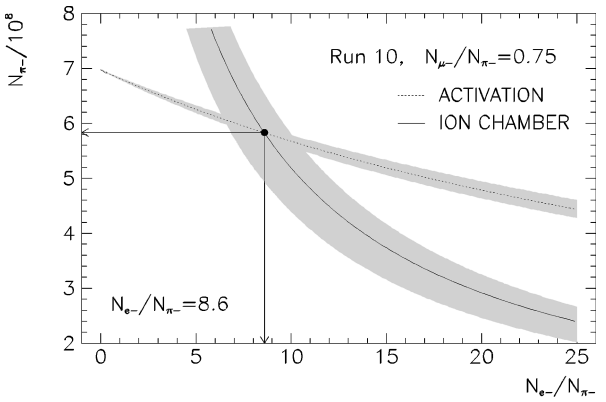

FIG. 1. The total number of beam π^-'s deduced from the number of ion chamber counts (full line) and the activation measurement (dotted line) as a function of the beam electron fraction N_{e^-}/N_{π^-} for one representative run. The μ^- contamination affects significantly only the ion chamber counts. Using six independent activations and fixing the N_{μ^-}/N_{π^-} ratio at 0.75 (see text) we find the e^- fraction of 8.7 ± 1.5, in good agreement with the *LAMPF User's Handbook* [19]. The shaded bands demonstrate the uncertainties of the π^-, e^-, and μ^- activation cross sections and the accuracy with which the ionization losses were known.

The ion chamber scaler counting rate was proportional to the factor

$$N_{\pi^-}(\Delta E_{\pi^-}+f_{e^-}\Delta E_{e^-}+f_{\mu^-}\Delta E_{\mu^-}), \tag{2.2}$$

where the ΔE_{π^-}, ΔE_{e^-}, and ΔE_{μ^-} corresponded to the π^-, e^-, and μ^- energy losses in the ion chamber gas. The activation measurements and ion chamber scaler counts were used simultaneously to deduce the beam electron fraction f_{e^-}. The value of the beam electron fraction, calculated by interpolation from the *LAMPF User's Handbook* Table 6A-VII [19] for the 27.5 MeV LEP π^- beam with the detectors located 2.5 m from the channel exit quadrupole, was $N_{e^-}/N_{\pi^-}=8.7$. Fixing the μ^- fraction at $N_{\mu^-}/N_{\pi^-}=0.75$, consistent with online observations, gave the measured f_{e^-} of 8.7 ± 1.5 (the quoted error is the standard deviation deduced from six independent activations). Varying the μ^- fraction between the outer limits of $f_{\mu^-}=0.5$ and 1.5 changes the overall beam flux normalization only weakly, by $\sim$3.3%. An example of the pion flux analysis for one representative activation data set is shown in Fig. 1.

The LEP channel is characterized by a background neutron flux of about $5\times10^{-4}n/\pi^-$. The contribution of this background to ^{11}C activation via the reaction ^{12}C$(n,2n)$ ^{11}C was estimated to be $\leqslant$0.5% in Ref. [13].

The total correction to the number of ''observed π^-'s,'' due to nonpionic contamination, amounted to 9.3%. The overall systematic uncertainty of the π^- flux normalization was 7.4% which reflects uncertainties in the ^{11}C activation cross sections, reproducibility, and systematic uncertainties of our activation measurement method, as well as uncertainties of the electron and muon beam fractions.

III. TARGETS

The LAMPF π^0 spectrometer [20] was used to detect π^0's produced in single charge exchange reactions on solid

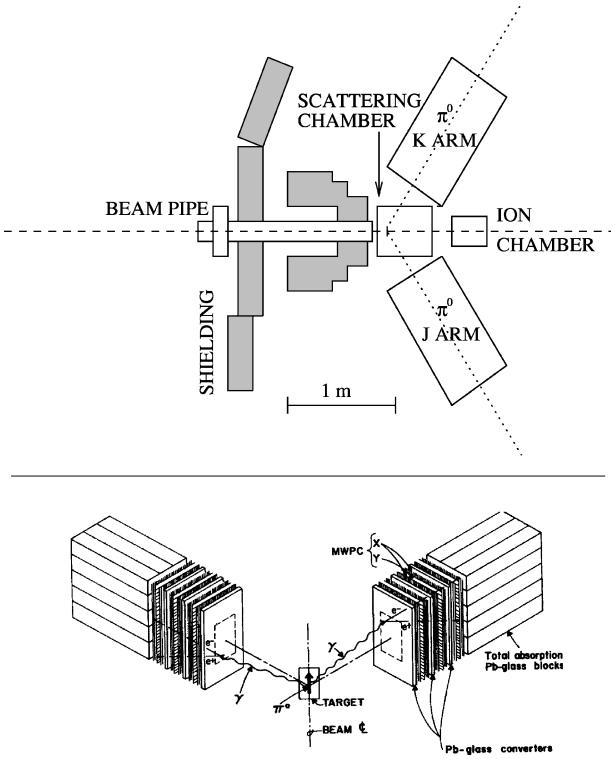

FIG. 2. Layout of the LEP experimental channel for the present experiment (top view) showing the arrangement of the π^0 spectrometer arms for an opening angle of 118° that optimizes the acceptance of the 25 MeV π^0's, as well as the scattering chamber, ion chamber, beam pipe, and shielding walls. The bottom panel is a schematic drawing of the π^0 spectrometer from Ref. [20]. The orientation of J and K arms in the two post configuration is shown. The details of the spectrometer arms, with three sets of converter, scintillator, and MWPC detectors, as well as the 3×5 array of lead-glass total absorption blocks can be seen.

CH_2 and ^{12}C targets, as well as on three different, thin-walled liquid hydrogen (LH_2) targets. The schematic layout of the experimental area is shown in Fig. 2. The target properties are summarized in Table II. Density nonuniformities of the solid targets were determined to be $\leqslant$1%.

Solid targets were mounted in air without use of an evacuated scattering chamber. They were oriented perpendicular to the beam direction with upstream faces positioned at the π^0 spectrometer pivot point. This geometry improved the π^0 energy resolution due to the partial compensation of the π^0 vertex uncertainty by the beam pion energy loss in the target.

The liquid H_2 target cell and the scattering chamber surrounding it were designed relying on insights gained in the analysis of data collected from two different, cylindrical Mylar target cells during initial test runs. The final target cell was a spherical copper flask with uniform wall thickness of 5.0 ± 1.3 μm. Fully filled with liquid H_2 the cell presented 142.4 ± 4.4 mb^{-1} of hydrogen to the incident pion beam.

The LH_2 scattering chamber was shaped in the form of a drum with an outer diameter of 55.9 cm and a 50.8 cm long horizontal axis aligned perpendicular to the beam direction. The cylindrical wall of the drum was made of 1.3 cm thick aluminum. Windows for beam entry and exit were cut in the walls of the cylinder and covered with a 25 μm thick Mylar band wrapped completely around the cylinder to preserve

TABLE II. List of targets used in the SCX measurements. For liquid hydrogen (LH_2) targets the geometrical diameters of cylindrical and spherical cells are quoted. Neutral pion yields measured with ^{12}C targets in the π^- beam were used to subtract the carbon contribution in CH_2 target data.

Target (Symbol)	Description	Thickness (mm)	Areal density (g/cm^2)	Areal density (mb^{-1})	Volume density (g/cm^3)
^{12}C ''A''	Graphite Sheet	3.18 ± 0.02	0.5289 ± 0.0040	26.54 ± 0.17	1.660
^{12}C ''B''	Graphite Sheet	6.82 ± 0.02	1.0787 ± 0.0045	54.13 ± 0.35	1.582
^{12}C ''C''	Graphite Sheet	3.40 ± 0.02	0.5374 ± 0.0023	26.97 ± 0.17	1.581
^{12}C ''D''	Graphite Sheet	4.95 ± 0.02	0.7826 ± 0.0050	39.27 ± 0.25	1.581
CH_2	Polyethylene Plate	7.77 ± 0.01	0.7112 ± 0.0020	91.77 ± 0.26	0.920
LH_2 ''A''	Vert. Mylar Cyl.	ø38.1 ± 1.0	0.247 ± 0.007	149.2 ± 4.6	0.070
LH_2 ''B''	Horiz. Mylar Cyl.	ø38.1 ± 1.0	0.214 ± 0.006	129.3 ± 4.0	0.070
LH_2 ''C''	Copper Sph. Bulb	ø38.1 ± 1.0	0.236 ± 0.006	142.4 ± 4.4	0.070

vacuum tightness. All detected photon pairs originating from low-energy π^0 decays in the target region ($T_{\pi^0}\leqslant 100$ MeV) passed through the chamber end plate windows. Each window consisted of a 13 μm thick Mylar sheet sandwiched between two Kevlar layers of the same thickness. On average, the window matter traversed by each photon was equivalent to 0.013 radiation lengths.

The mounted targets were surveyed with a transit theodolite and their position at the spectrometer pivot point was always confirmed independently to within ±1 mm by ^1H $(p,p)p$ scattering measurements. The incident proton beam spot was moved across the target in both the horizontal and vertical directions by varying the beam line bending magnet field values.

The effective thicknesses of the target cells presented to the beam particles and to the outgoing π^0 photons were calculated in a GEANT Monte Carlo simulation [21], Table II. These derived thicknesses were corrected subsequently for the fraction of the $\pi^0\rightarrow\gamma\gamma$ photons converting in the target material, scattering chamber, and spectrometer preradiators. f_a, the probability for absorption of either π^0 decay photon in material preceding the spectrometer converters, was calculated in the Monte Carlo simulation and depended on the selected experimental geometry and the target type; its values ranged from 12 to 36 %. Δf_a, the combined statistical and systematic uncertainty of the f_a values, was less than 1%.

The average incident π^- kinetic energies, integrated along the thickness of the CH_2 or liquid H_2 target and weighted with the π^- beam profiles and beam energy straggling, were 27.5 ± 0.2 and 26.4 ± 0.2 MeV, respectively. The absolute value of the beam central momentum in the LEP channel is known with a 0.5% accuracy. That uncertainty limit was set by measuring the energies of spallation particles created at the pion production target [22]. Beam momentum reproducibility was better than 10^{-4} owing to the uncertainties in NMR measurements of magnetic fields in the beam line bending magnets.

The upstream vacuum window of the scattering chamber was placed 16.5 cm upstream of the target. Consequently, the LH_2 target location was 11.5 cm upstream of the scattering chamber center. This design reduced the background rates from SCX events in air by 40%. Extensive shielding of an upstream section of the LEP beam line suppressed accidental background rates in the π^0 detector to $\leqslant2\%$ of the π^0 signal (Fig. 3).

IV. π^0 DETECTION: ACCEPTANCE AND EFFICIENCY

The data were taken with the π^0 spectrometer in the ''two-post'' configuration [23], with two arms (labeled J and K, respectively) positioned symmetrically left and right with respect to the incident π^- beam (Fig. 2). Two different scattering polar angles were selected for data taking, 0° and 20°, with a 118° opening angle between the two spectrometer arms and the 55 cm nominal detector-to-target distance. This configuration is optimized for maximum geometrical acceptance of two coincident photons following the decay of a 25 MeV π^0. The spectrometer's multiwire proportional chambers' (MWPC's) fiducial cuts imposed in the analysis required a reconstructed photon conversion vertex in the spectrometer lead glass detectors to lie within a pyramidal volume whose apex coincides with the target center and whose base is a rectangle located two radiation lengths deep

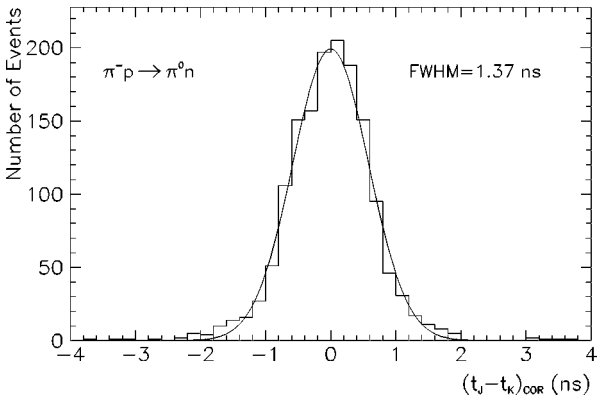

FIG. 3. Histogram of relative timing between the two arms (J and K) of the LAMPF π^0 spectrometer for the π^0 SCX events on the CH_2 target at 27.5 MeV. TDC values for the scintillator planes in J and K arms were corrected for the photon time-of-flight between the event target vertex and photon conversion points as well as for the light propagation delay in the scintillator planes. The achieved timing resolution was 1.37 ns FWHM. The crucial feature is the absence of an accidental background: virtually all events ($\geqslant98\%$) in the histogram are real π^0's.

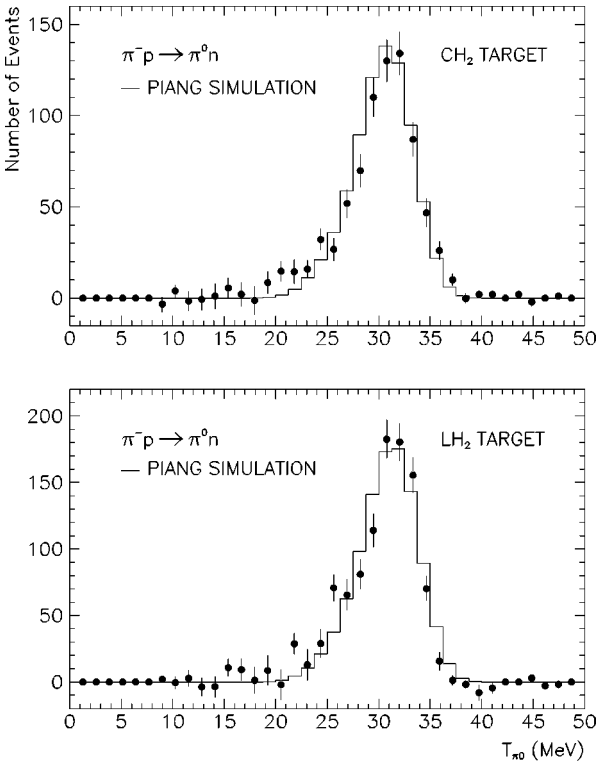

FIG. 4. The net subtracted π^0 kinetic energy spectra for the single charge exchange reaction on the proton at 27.5 and 26.4 MeV, respectively. Top panel shows the data obtained with the 0.711 g/cm^2 thick CH_2 target. The ^{12}C contribution was measured and corrected for by measuring the π^0 yield from an equivalent-thickness carbon target. The bottom panel shows the spectrum acquired with the 0.236 g/cm^2 liquid hydrogen target (LH_2 ''C'' in Table II). Solid histograms represent results of Monte Carlo calculations of the π^0 spectrometer acceptance with the modified PIANG code [23]. The γ-γ energy asymmetry cut $X=(E_J-E_K)/(E_J+E_K)\leq 0.2$ was applied to both measured and simulated events.

in the spectrometer calorimeter blocks extending to the calorimeter edges. The detector acceptance for monoenergetic π^0's with the nominal incident kinetic energy of 30 MeV was calculated with the Monte Carlo program PIANG [23] and the results are listed in Table IV. Essentially the same effective solid angle values were obtained in a GEANT model of the detector response. Comparing the PIANG and GEANT calculations leads to an estimated 3% systematic uncertainty of the π^0 angular acceptance. The uncertainty is dominated by electromagnetic losses near the margins of the fiducial areas. The energy line shapes of the detected π^0's from CH_2 and liquid H_2 targets are compared to the simulated π^0 energy spectra in the two panels of Fig. 4.

The π^0 spectrometer detection efficiency is an important factor in determining the overall uncertainty of the cross sections because of the complexity of the instrument. In the past, the spectrometer instrumental efficiency was calibrated to about 1% accuracy at the π^- beam momentum of 522 MeV/c [24], but it is significantly less well understood at the low momenta used in the present work.

We used penetrating cosmic muons to measure directly the intrinsic instrumental efficiencies of the lead glass detectors, plastic scintillator elements, and the multiwire proportional chambers. J and K arm calibrations were performed

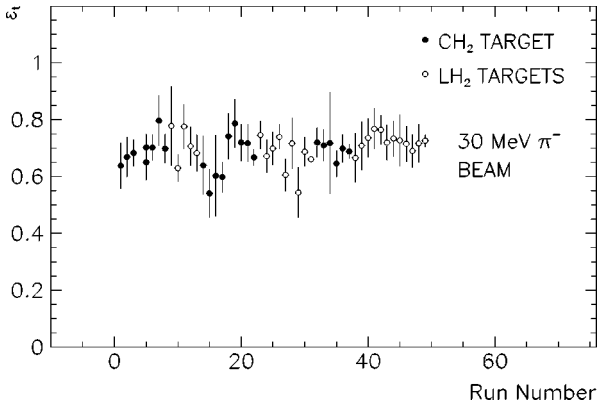

FIG. 5. The average tracking efficiency ϵ_t calculated for all SCX runs was 0.76 ± 0.02. The data collected with the solid CH_2 target as well as with the liquid H_2 targets were included in the quoted average. The absence of accidental backgrounds implies constant ϵ_t, independent of the detector geometry and influenced only by the tracking cuts used in the analysis. The data points confirm that expectation.

independently, collecting $\geq 10^5$ cosmic muon events in each arm, resulting in approximately a 0.3% statistical uncertainty in the deduced detector efficiencies.

The spectrometer π^0 detection efficiency ϵ_{π^0} can be decomposed into a product of individual efficiencies [25]:

$$\epsilon_{\pi^0}=\epsilon_{\pi^0}^{JK}\epsilon_m\epsilon_c\epsilon_s\epsilon_t\epsilon_b, \tag{4.1}$$

where $\epsilon_{\pi^0}^{JK}$ is the simultaneous conversion probability for both $\pi^0\rightarrow\gamma\gamma$ decay photons in the J and K arms, ϵ_m is the weighted combined wire chamber efficiency, ϵ_c is the converter ''transparency'' for the charged showers (defined below), ϵ_s is the weighted scintillator efficiency for minimum ionizing particles (MIP's), ϵ_t represents the tracking algorithm efficiency for the accepted photon showers, and ϵ_b is a small correction due to the shower back splash. Some of these efficiencies depend weakly on the π^0 kinetic energy and direction, the γ-γ energy asymmetry and the photon conversion point positions. These dependencies were studied and have been taken into account in the GEANT simulations of the spectrometer response described in the following text.

The two-photon conversion probability $\epsilon_{\pi^0}^{JK}$ is a function of the single converter plane conversion probability ϵ_γ:

$$\epsilon_{\pi^0}^{JK}=[1-(1-\epsilon_\gamma)^3]^2. \tag{4.2}$$

The quantity ϵ_γ was extracted directly from our data in an offline analysis of all recorded πp SCX events. The π^0 events at the π^- incident energy of 27.5 MeV involved detection of coincident photon pairs with each γ having the energy of $E_\gamma\simeq 82$ MeV. The distribution of triggered conversion plane pairs was tabulated in a 3×3 matrix. Each entry in the matrix corresponded to the number of good photon conversions in a given (J,K) pair of arm converter planes. The efficiency ϵ_γ was then calculated in a simultaneous fit to all nine matrix elements.

The value ϵ_γ has also been previously determined semiempirically by the equation [20]

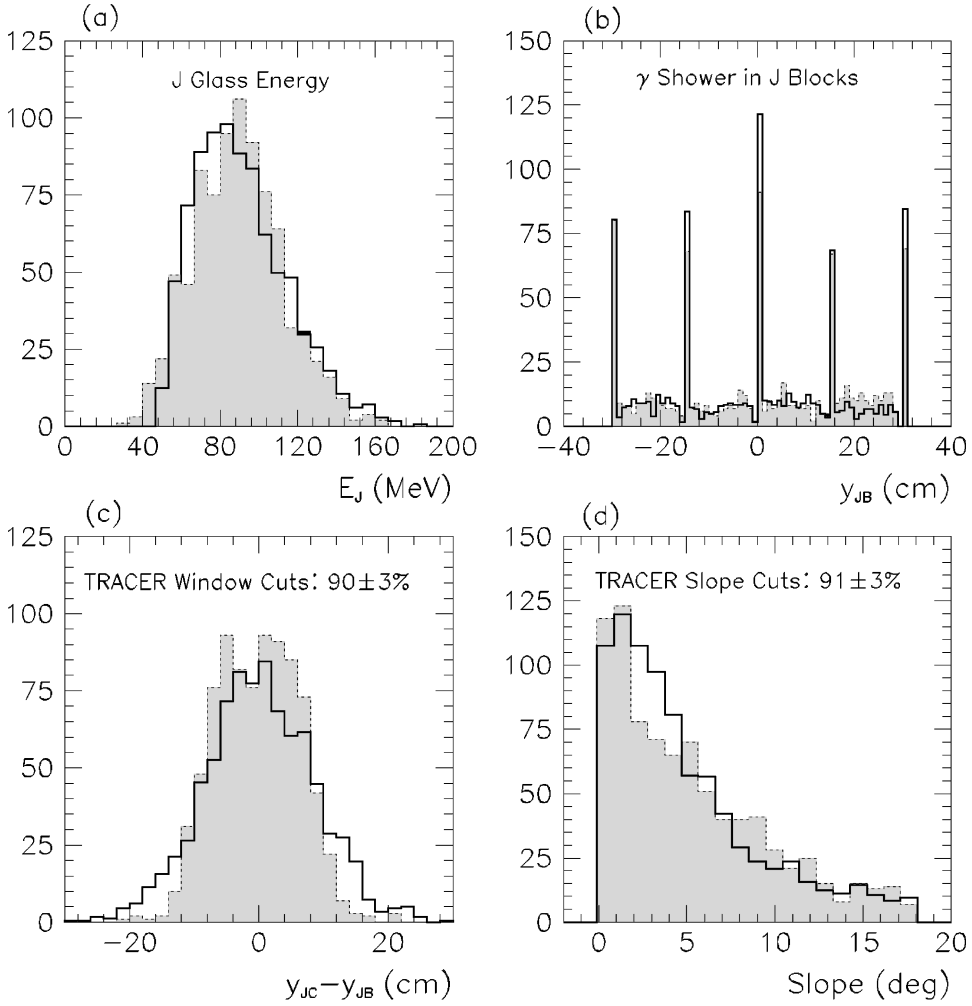

FIG. 6. A GEANT simulation of the tracking efficiency of the π^0 spectrometer analyzer code. Neutral pions generated from 27.5 MeV π^- beam SCX interactions in the CH_2 target were identified by the electromagnetic showers tracked through the volume of the modeled spectrometer arm. On average, the showers produced 1.37 charged minimum-ionizing particles exiting the converter. The percentage of the two-arm π^0 decay photon conversions surviving the TRACER window and slope cuts on the reconstructed trajectories and passing a limit on the maximum number of hit wires in this simulation was $73\pm3\%$. That result should be compared with the measured tracking efficiency of $76\pm2\%$. The panels show (a) measured (full histogram) and simulated (shaded histogram) energy spectra in a lead glass calorimeter, (b) a distribution of the energy-weighted coordinates of the hit blocks in the segmented 3×5 element lead glass calorimeter, (c) differences between the coordinates of a MWPC-reconstructed γ conversion point and the energy-weighted lead block energy deposition location, and (d) measured and simulated ''best'' angle between the back-projected line from the target center to the conversion point deduced from hits in X and X' wire chambers and to a shower's center-of-gravity in lead-glass blocks. All histograms (measured or simulated) shown in the four panels correspond to ''good'' π^0 events only.

$$\epsilon_\gamma = 0.86\{0.327 + 0.1\log_{10}[0.01E_\gamma\,(\mathrm{MeV})]\}, \qquad (4.3)$$

with parameters based on photon interaction probabilities [26] and the known converter specifications. The above relation, Eq. (4.3), places ϵ_γ just 2.5 standard deviations below our measured value of 0.292 ± 0.006.

The analyzed event fraction η_a, defined as the ratio of the number of π^0 hardware triggers to the number of ''analyzable'' events with good wire chamber information, was understood entirely in terms of the instrumental MWPC efficiencies. Over the period of the experiment, for each individual run, η_a was equal (within the associated statistical uncertainty) to the appropriately weighted product of six intrinsic wire chamber efficiencies. The average efficiency $\epsilon_m^{1/6}$ of a single MWPC chamber varied between 94.4 and 95.6 % over one month of data collection. The average veto counter and scintillator counter efficiencies, $\epsilon_v^{1/2}$ and $\epsilon_s^{1/2}$, appropriately weighted with photon conversion probabilities in three conversion planes, were calculated to be 96.9 and 96.1 %, respectively.

The efficiency of the electromagnetic shower tracking algorithm was extracted independently from the 27.5 MeV SCX runs with LH_2 and CH_2 targets, after subtraction of the appropriate target-empty and ^{12}C target backgrounds from the data. The ratio of the number of events which survived all analyzer cuts to the number of events that satisfied less restrictive conditions for good MWPC hits inside predefined fiducial areas, was defined as the tracking efficiency ϵ_t. The measured tracking efficiency was stable for all collected data sets and averaged 0.76 ± 0.02, as demonstrated in Fig. 5.

TABLE III. Factors contributing to the total π^0 detection efficiency given by the integral value $\int \epsilon_{\pi^0} d\Omega_{\pi^0} dT_{\pi^0} = 0.175 \pm 0.008$. The measurement [23] is scaled down for the new thinner converters but corresponds to 100 MeV photons as compared to lower-energy gammas from our Monte Carlo simulation ($\sim$82 MeV γ's from 27.5 MeV π^0's decays). The uncertainties listed in the fifth column are the combinations of statistical and estimated systematic (when applicable) standard deviations.

Symbol	Description	Method	Efficiency (%)	Error (%)
ϵ_γ	single converter detection efficiency	SCX π^0 detection [25]	29.2	2.0
		γ attenuation coefficients [26]	27.9	1.0
ϵ_m	instrumental MWPC efficiency	cosmic muon trigger [25]	78.8	0.2
ϵ_c	converter transparency for	GEANT simulation [25]	88.9	0.4
	minimum ionizing particles	experiment [23]	87.6	1.0
ϵ_s	weighted scintillator efficiency	cosmic muon trigger [25]	92.5	0.5
ϵ_p	maximum number of	cosmic ray trigger+SCX [25]	92.4	1.0
	charged particle prongs	tagged γ beam [23]	91.4	2.0
ϵ_d	TRACER shower window cuts	GEANT simulation [25]	73.0	3.0
		SCX π^0 detection [25]	76.0	2.0
ϵ_v	weighted veto efficiency	cosmic muon trigger [25]	93.9	0.5
ϵ_b	backsplash self-vetoing	GEANT code [25]	98.8	0.2

All relevant instrumental and software aspects of π^0 detection in the spectrometer were studied in a complementary way and in greater detail in a GEANT simulation [21] in order to provide a cross check for the measured efficiencies. In this simulation the required material properties of Schott LF5 lead glass (of which the converters and total absorption blocks are made), were taken from the original manufacturer's specification [27]. The Monte Carlo calculation yielded a $29.2 \pm 2.0\%$ single-plane conversion efficiency. An event was counted as a ''good'' π^0 γ conversion if a photon, interacting in the converter material by the photoelectric effect, Compton scattering, or pair production, generated secondary particles that deposited more than 50 MeV in the lead glass calorimeter. The same energy threshold for a single spectrometer arm was used in the data analysis. The agreement between measured and simulated probabilities quoted above confirms that we had specified the appropriate converter composition and analysis cuts.

Simulated showers that converted into neutral events inside the converter or events that failed to provide the necessary tracking pulses in scintillators and wire chamber planes had to be taken into account separately. The probability that a photon from π^0 decay generates a shower with at least one detectable charged particle in the volume occupied by the MWPC planes defined the converter transparency $\epsilon_c^{1/2}$. In high-statistics simulations, opacity, i.e., the inefficiency of shower tagging $(1-\epsilon_c^{1/2})$, converged to a value of $5.6 \pm 0.2\%$. This probability should be compared with the previous converter opacity measurement of $7.2 \pm 0.5\%$ for 15% thicker converters [28].

Particularly important for the determination of tracking efficiency were tests imposed in the analyzer TRACER routine which reconstructed the trajectories of the charged shower particles through a spectrometer arm. The TRACER tracking reconstruction was simulated in the GEANT GUSTEP subroutine where shower particles were tracked through all elements of the experimental apparatus. Efficiency parameters, relating the response of the wire chambers to the minimum ionizing particles, were inferred from the high-statistics cosmic muon measurements. The following cuts were implemented.

(i) The photon shower coordinates were reconstructed independently from (a) the MWPC wires that were hit, and (b) from the shower energy distribution inside the calorimeter lead glass blocks. Both sets of coordinates were projected back to the scintillator plane immediately following the conversion plane where the shower originated. The two projected points were required to fall inside an acceptance window of $\Delta x \times \Delta y = 10 \times 20$ cm.

(ii) After photon conversion the electromagnetic shower is tracked through at least two wire chamber planes. On the basis of the resulting MWPC wire hits a shower track direction was reconstructed. This direction was compared with the line connecting the target center and the conversion point (defined above). The relative angle between the two lines was required to be $\leqslant 18°$.

(iii) If in the tracking of a shower any individual MWPC plane reported more than four wires hit, the event was discarded.

These cuts were identical to the ones imposed in the data analysis. The tracking efficiency ϵ_t deduced from the percentage of simulated $\pi^0 \rightarrow \gamma\gamma$ photon conversions surviving all analyzer cuts was 0.73 ± 0.03, where most of the uncertainty is due to approximations involved in the Monte Carlo description of the MWPC geometry and response. The Monte Carlo value is in good agreement with the experimental value $\epsilon_t = 0.76 \pm 0.02$ listed above. The latter value was used in the calculation of the differential cross sections (see also Figs. 5 and 6).

In summary, the detection efficiency of the π^0 spectrometer was calibrated for the photon energy range 50–100 MeV with a 4.6% uncertainty. The ingredients entering the detection efficiency calculation are summarized in Table III. The integrated value of ϵ_{π^0} for our spectrometer settings and choice of adjustable analyzer cuts was 0.175 ± 0.008. The general approach outlined in this section, however, can be

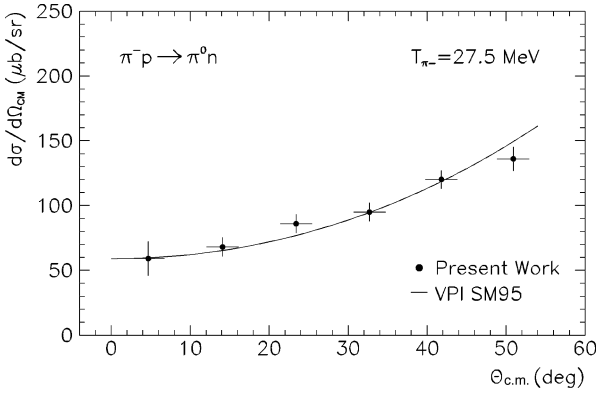

FIG. 7. Measured differential cross sections for the $\pi^- p \rightarrow \pi^0 n$ reaction at 27.5 ± 0.2 MeV. The plotted cross sections were obtained by subtracting the measured ^{12}C contribution from the π^0 yields with the CH_2 target. The plotted error bars are statistical uncertainties only, calculated from numbers of detected events. In addition, an overall normalization uncertainty of 8.7% applies to all points (see text). The full line represents the VPI SM95 πp SCX partial-wave solution [1].

followed to calculate or measure the spectrometer detection efficiency for any chosen set of applied tests as well as for different π^0 energies.

V. RESULTS AND DISCUSSION

Collecting the results presented in Secs. II–IV, single charge exchange differential cross sections were evaluated for six 8° wide polar angle bins. The acceptable angular bin sizes were restricted by the 5.5° rms directional resolution of the spectrometer and by the event statistics. The variation of the cross section over the range of pion energies present in the target (due to the combination of nonzero π^- beam momentum spread and π^- energy loss in the target) was taken into account by assuming the cross section energy dependence of the VPI SM95 partial-wave solution [1]. This cross section scaling correction f_σ was bracketed within the $(-0.5\%, +1.0\%)$ range and all extracted cross sections were referred to the central beam on-target energy of 27.5 MeV.

The differential cross sections were calculated using the expression

$$\frac{d\sigma}{\Delta\Omega}(\theta_{\text{c.m.}}) = \frac{YJf_\sigma}{N_{\pi^-} t \Delta\Omega_{\pi^0} \epsilon_{\pi^0} (1-f_a) \Gamma_{\pi^0 \rightarrow \gamma\gamma} \eta_c \eta_v}, \tag{5.1}$$

where Y is the number of detected π^0's in a given angular bin after background subtraction, J is the Jacobian of transformation from the laboratory (lab) to the center-of-momentum (c.m.) frame, f_σ is the factor defined just above, N_{π^-} is the number of beam π^-'s incident on a target, t is the effective target thickness, $\Delta\Omega_{\pi^0}$ is the laboratory solid angle of an angular bin, ϵ_{π^0} is the integrated π^0 detection efficiency for a given bin, $(1-f_a)$ is the fraction of photons not absorbed before conversion, $\Gamma_{\pi^0 \rightarrow \gamma\gamma}$ is the $\pi^0 \rightarrow \gamma\gamma$ decay branching ratio, η_c is the computer live time fraction, and η_v is the spectrometer veto live time fraction.

The experimental angular distribution is plotted in Fig. 7 and results are summarized in Table IV, together with the comparison with the results of the latest pion-nucleon phase-shift analysis by the VPI group SM95 [1]. Using the analysis presented here, our experimental yields lead to differential cross sections that are 1.01 ± 0.06 times the VPI SM95 partial-wave solution in the angular range covered, $\theta = 0° - 55°$. The overall normalization uncertainty of the experiment 8.7% is due to the 7.4% uncertainty in the pion flux (Sec. II) and the 4.6% uncertainty of ϵ_{π^0}, the π^0 spectrometer detection efficiency (Sec. IV). Combining the statistical and systematic uncertainties of the data points we find all our measurements fall within one standard deviation of the partial-wave predictions. While the πN amplitude analysis has been plagued by inconsistencies in the experimental data base below about 150 MeV since the 1980's, our results confirm the validity of the ''standard'' pion-nucleon phase shift analysis in the important low-energy region. Incorporation of our data points, which have smaller combined statistical and systematic uncertainties then the previous forward-angle measurements, into the low-energy SCX database will have a constraining influence on future partial-wave analyses.

We note that the similar low-energy measurement of Fitzgerald *et al.* [10], performed with the same instrument, should be corrected with the new and more precise ^{11}C activation cross sections [16]. Thus a ''minimal'' correction to the differential cross sections of Fitzgerald *et al.* at 32.5

TABLE IV. Experimental differential cross sections for the πp SCX reaction at 27.5 ± 0.2 MeV, measured using the CH_2 target with hydrogen thickness of 0.0612 g/cm^2. The comparison with the VPI partial-wave analysis SM95 [1] is shown in the last column. The quoted error bars are statistical uncertainties from the measured yields, background count subtractions, and Monte Carlo acceptance statistics. There is an additional overall 8.7% systematic uncertainty, due to the pion flux normalization and π^0 spectrometer detection efficiency (see text). It applies to all six measured cross sections.

$\langle \cos\theta_{\text{c.m.}} \rangle$	Yield Y	$\Delta\Omega_{\text{c.m.}}$ (msr)	$d\sigma/d\Omega\|_{\text{c.m.}}$ (μb/sr)	$\frac{d\sigma/d\Omega\|^{\text{E1179}}_{\text{c.m.}}}{d\sigma/d\Omega\|^{\text{SM95}}_{\text{c.m.}}}$
0.99664	37.3 ± 8.4	2.338 ± 0.011	59 ± 13	0.99 ± 0.23
0.96998	129.2 ± 14.5	6.994 ± 0.020	68 ± 7	1.04 ± 0.12
0.91769	254.2 ± 19.6	10.967 ± 0.024	86 ± 7	1.12 ± 0.09
0.84173	311.7 ± 21.5	12.163 ± 0.026	95 ± 7	1.00 ± 0.07
0.74494	304.5 ± 20.5	9.644 ± 0.023	120 ± 7	1.00 ± 0.06
0.63070	211.5 ± 15.4	5.772 ± 0.017	136 ± 9	0.91 ± 0.06

MeV would imply a renormalization factor of 1.48 (Table I, fifth column). This procedure would make the existing disagreement (about one standard deviation) with the VPI SM95 πp SCX partial wave solution even worse. However, as insufficient details are given in Ref. [10] regarding the extraction of the pion fraction in the beam, the appropriate correction procedure may be more involved. Finally, in view of our comprehensive analysis of the π^0 detection efficiency, we suggest that the corresponding part of the analysis of Fitzgerald *et al.* should be refined.

ACKNOWLEDGMENTS

We thank the staff of LAMPF groups MP-7 and MP-8 for strong technical support, without which our measurements would not have been possible. We are particularly indebted to Bob Garcia who was responsible for the liquid hydrogen target design and construction. We acknowledge fruitful discussions with M. Sadler. This work was supported by the U.S. National Science Foundation and U.S. Department of Energy.

[1] R. A. Arndt, I. I. Strakovsky, R. L. Workman, and M. M. Pavan, Phys. Rev. C **52**, 2120 (1995).
[2] R. A. Arndt, Z. J. Li, L. D. Roper, R. L. Workman, and J. M. Ford, Phys. Rev. D **43**, 2131 (1991).
[3] W. R. Gibbs, L. Ai, and W. B. Kaufmann, Phys. Rev. Lett. **74**, 3740 (1995).
[4] P. B. Siegel and W. R. Gibbs, Phys. Rev. C **33**, 1407 (1986).
[5] J. Gasser and H. Leutwyler, Phys. Rep. **87**, 77 (1982).
[6] R. Koch, J. Phys. C **15**, 161 (1982).
[7] J. Gasser, H. Leutwyler, and M. Sainio, Phys. Lett. B **253**, 252 (1991).
[8] M. Salomon, D. F. Measday, and J-M. Poutissou, Nucl. Phys. **A414**, 493 (1984).
[9] A. Bagheri, K. A. Aniol, F. Entezami, M. D. Hasinoff, D. F. Measday, J-M. Poutissou, M. Salomon, and B. C. Robertson, Phys. Rev. C **38**, 885 (1988).
[10] D. H. Fitzgerald, H. W. Baer, J. D. Bowman, M. D. Cooper, F. Irom, N. S. P. King, M. J. Leitch, E. Piasetzky, W. J. Briscoe, M. E. Sadler, K. J. Smith, and J. N. Knudson, Phys. Rev. C **34**, 619 (1986).
[11] M. E. Sadler, B. M. Brooks, L. D. Isenhower, W. J. Briscoe, J. D. Bowman, D. H. Fitzgerald, and J. N. Knudson, πN Newsletter **4**, 131 (1991).
[12] R. L. Burman, R. L. Fulton, and M. Jakobson, Nucl. Instrum. Methods **131**, 29 (1975).
[13] G. W. Butler, B. J. Dropesky, C. J. Orth, R. E. L. Green, R. G. Korteling, and G. K. Y. Lam, Phys. Rev. C **26**, 1737 (1982).
[14] D. Počanić, E. Frlež, K. A. Assamagan, J. P. Chen, K. J. Keeter, R. M. Marshall, R. C. Minehart, L. C. Smith, G. E. Dodge, S. S. Hanna, B. H. King, and J. N. Knudson, Phys. Rev. Lett. **72**, 1156 (1994).
[15] W. R. Leo, *Techniques for Nuclear and Particle Physics Experiments* (Springer-Verlag, New York, 1987), p. 24, and references therein.
[16] M. J. Leitch (private communication); LAMPF Experiment E942, 1992.
[17] G. Kuhl and U. Kneissl, Nucl. Phys. **A195**, 559 (1972).
[18] C. J. Orth, M. W. Johnson, J. D. Knight, and K. Wolfsberg, LAMPF Experiment E331, 1977.
[19] H. Howard, *LAMPF User's Handbook*, MP-DO-1-UHB, 3rd ed. (LANL, Los Alamos, 1987).
[20] H. W. Baer, R. D. Bolton, J. D. Bowman, M. D. Cooper, F. H. Cverna, R. H. Heffner, C. M. Hoffman, N. S. P. King, J. Piffaretti, J. Alster, A. Doron, S. Gilad, M. A. Moinester, P. R. Bevington, and E. Winkelmann, Nucl. Instrum. Methods **180**, 445 (1981).
[21] R. Brun, F. Bruyant, M. Maire, A. C. McPherson, and P. Zanarini, GEANT3, CERN Report No. DD/EE/84-1, 1987.
[22] M. V. Hoehn and D. H. Fitzgerald, LAMPF Report No. A82-01, 1982.
[23] S. Gilad, Ph. D. thesis, Tel Aviv University, 1979.
[24] F. C. Gaille, V. L. Highland, L. B. Auerbach, W. F. McFarlane, G. E. Hogan, C. M. Hoffman, R. J. Macek, R. E. Morgado, J. C. Pratt, and R. D. Werbeck, Phys. Rev. D **30**, 2408 (1984).
[25] E. Frlež, Ph. D. Thesis, University of Virginia, 1993; LANL Report No. LA-12663-T, 1993.
[26] J. H. Hubbel, *Photon Cross Sections, Attenuation Coefficients, and Energy Absorption Coefficients from 10 keV to 100 GeV* (NBS Publ. NSRDS-NBS, 1969), Vol. 29, p. 1.
[27] H. W. Baer, *The π^0 Spectrometer Notes* (LANL, Los Alamos, 1980).
[28] S. Gilad, J. D. Bowman, M. D. Cooper, R. H. Heffner, C. M. Hoffman, M. A. Moinester, J. M. Potter, F. H. Cverna, H. W. Baer, P. R. Bevington, and M. W. McNaughton, Nucl. Instrum. Methods **144**, 103 (1977).
[29] B. J. Dropesky, G. W. Butler, C. J. Orth, R. A. Williams, M. A. Yates-Williams, G. Friedlander, and S. B. Kaufman, Phys. Rev. C **20**, 1844 (1979).